ETH

Eidgenössische Technische Hochschule Zürich
Swiss Federal Institute of Technology Zurich

Coupling Finite Elements and Auxiliary Sources for Maxwell's Equations

D. Casati and R. Hiptmair and J. Smajic

Coupling Finite Elements and Auxiliary Sources for Maxwell's Equations

Daniele Casati*[1] | Ralf Hiptmair[1] | Jasmin Smajic[2]

[1]Seminar for Applied Mathematics, ETH Zurich, Zurich, Switzerland

[2]Institute for Energy Technology, Hochschule für Technik Rapperswil, Zurich, Switzerland

Correspondence
*Daniele Casati, Email: daniele.casati@sam.math.ethz.ch

Present Address
Seminar for Applied Mathematics, ETH Zurich, Zurich, Switzerland

Summary

The Multiple Multipole Program is a Trefftz method approximating the electromagnetic field in a domain filled with a homogeneous linear medium. MMP can easily cope with unbounded domains; yet, it cannot accommodate either inhomogeneous or nonlinear materials, situations well within the scope of the standard Finite Element Method.

We propose to couple FEM and MMP to model Maxwell's equations for materials with nonlinear local properties in an unbounded domain. In some bounded parts of the domain, we use Nédélec's first family of curl-conforming elements; in the unbounded complement, multipole expansions. Several approaches are developed to couple both discretizations across the common interface:

1. Least-squares-based coupling using techniques from PDE-constrained optimization.

2. Multi-field variational formulation in the spirit of mortar finite element methods.

3. Discontinuous Galerkin between the FEM mesh and the single-entity MMP subdomain.

4. Coupling through tangential components traces.

We study the convergence of these approaches in a series of numerical experiments.

KEYWORDS:
finite element method, multiple multipole program, method of auxiliary sources, Trefftz method, computational electromagnetics

1 | INTRODUCTION

We consider the following second-order vector elliptic boundary value problem that expresses a magnetostatic regime in vector potential formulation:

$$\begin{cases} \nabla \times [\mathbf{M}(\mathbf{x}) \, \nabla \times \mathbf{u}] + \nabla \phi = \mathbf{f} \\ -\nabla \cdot \mathbf{u} = 0 \end{cases} \quad \text{in } \mathbb{R}^3, \tag{1a}$$

$$\mathbf{u}(\mathbf{x}) = \mathcal{O}\left(\|\mathbf{x}\|^{-1}\right) \quad \text{for } \|\mathbf{x}\| \to \infty \text{ uniformly.} \tag{1b}$$

- $\mathbf{M} : \mathbb{R}^3 \to \mathbb{R}^{3,3}$ is a symmetric, bounded, uniformly positive-definite material coefficient. We assume that $\mathbf{M}$ agrees with the identity matrix $\mathbf{I} \in \mathbb{R}^{3,3}$ outside of a bounded domain $\Omega_\star$:

$$\Omega_\star \subset \mathbb{R}^3 : \mathbf{M}(\mathbf{x}) = \mathbf{I} \quad \forall \mathbf{x} \in \mathbb{R}^3 \setminus \Omega_\star. \tag{2}$$

---

[0]**Abbreviations:** FEM: Finite Element Method. MMP: Multiple Multipole Program. Index f in formulas: FEM. Index m in formulas: MMP. PDE: Partial Differential Equation. DG: Discontinuous Galerkin.

- $\mathbf{u} : \mathbb{R}^3 \to \mathbb{R}^3$ represents the vector magnetic potential. The former equation in (1a) is the Ampère's law, the latter the Coulomb gauge.

- $\phi : \mathbb{R}^3 \to \mathbb{R}$ is a Lagrange multiplier to impose the Coulomb gauge. ϕ must be subject to a further constrain such that it is uniquely defined by (1a). In the scope of this work, we set $\int_{\mathbb{R}^3} \phi \, \mathrm{d}\mathbf{x} = 0$.

- $\mathbf{f} : \mathbb{R}^3 \to \mathbb{R}^3$, with $\nabla \cdot \mathbf{f} = 0$, represents the static current that generates the magnetic field. $\mathbf{f}$ has compact support in $\Omega_\star$.

- For the decay condition (1b), please refer to [1, p. 180, (5.28)].

The weak solution $\mathbf{u} \in \mathbf{H}_{\mathsf{loc}}\left(\mathbf{curl}, \mathbb{R}^3\right)$ of (1) belongs to the continuous Trefftz space

$$\mathcal{T}\left(\mathcal{D}\right) := \left\{ \mathbf{v} \in \mathbf{H}_{\mathsf{loc}}\left(\mathbf{curl}, \mathcal{D}\right) : \ \nabla \times \nabla \times \mathbf{v} = \mathbf{0}, \ \nabla \cdot \mathbf{v} = 0, \ \mathbf{v} \text{ satisfies the decay condition (1b)} \right\} \tag{3}$$

for $\mathcal{D} = \mathbb{R}^3 \setminus \Omega_\star$.

Trefftz methods seek to approximate $\mathbf{u}$ on subdomains of $\mathbb{R}^3 \setminus \Omega_\star$ by means of some finite-dimensional subspace of $\mathcal{T}\left(\mathcal{D}\right)$. Our approach uses spaces spanned by multipole expansions that exhibit central singularities outside of $\mathcal{D}$. We refer to this discretization as the MMP approximation after the Trefftz method known as *Multiple Multipole Program*; see Section 2 for details.

However, functions in a Trefftz space cannot approximate $\mathbf{u}$ in $\Omega_\star$. There we use a standard finite element space $\mathbf{V}_{\mathsf{n}}$, $\mathbf{V}_{\mathsf{n}}|_{\Omega_\star} \subset \mathbf{H}\left(\mathbf{curl}, \Omega_\star\right)$, together with the usual primal variational formulation of (1).

The main issue arising is how to impose the coupling between the MMP domain and the finite element domain. Several algorithms will be presented in Section 3. Their convergence will be shown numerically in Section 4.1. We will discuss their complete numerical analysis in a next publication.

1.1 | Related Work

The coupling between FEM and MMP for the Poisson's equation has been discussed by the authors from the perspective of numerical analysis in [2]. The approaches we propose to realize the coupling have been described there for the first time, except for the approach of Section 3.3.

The FEM–MMP coupling has also been tackled before from an engineering perspective by one of the authors [3]. The numerical experiment proposed in that work is a 2-dimensional version of the model discussed here in Section 4.2. A different methodology for coupling FEM and MMP is used: coupling is done by ad-hoc point matching of field values, the Dirichlet data, on the interface between the FEM and MMP domains (*collocation method*), while the Neumann data enter through a boundary term of the variational formulation. The resulting overdetermined FEM–MMP system of equations is solved in the least-squares sense.

To the best of our knowledge, outside of these papers little work has been devoted to the investigation of strategies combining Trefftz methods with conventional finite element methods.

2 | MULTIPLE MULTIPOLE PROGRAM

The concept of the Multiple Multipole Program was proposed by Ch. Hafner in his dissertation [4] based on the much older work of G. Mie and I. N. Vekua [5, 6]. Essentially, the Mie-Vekua approach expands the field in a 2D multiply-connected domain by a multipole expansion supplemented with generalized harmonic polynomials. Extending these ideas, MMP introduces more multipoles (multiple multipoles) than required according to Vekua's theory [6].

2.1 | Multipoles

Basis functions spanning the MMP Trefftz spaces (3) are the so-called *multipoles*, potentials spawned by (anisotropic) point sources. Given (3), multipoles are exact solutions of the homogeneous system of PDEs $\nabla \times \nabla \times \mathbf{u} = \mathbf{0}$, $\nabla \cdot \mathbf{u} = 0$ subject to the decay condition (1b).

A multipole can be formulated as $\mathbf{v}\left(\mathbf{x}\right) := \mathsf{f}\left(r_{\mathsf{xc}}\right) \mathbf{g}\left(\theta_{\mathsf{xc}}, \varphi_{\mathsf{xc}}\right)$ in a spherical coordinate system in $\mathbb{R}^3$ ($r \in [0, \infty)$, $\theta \in [0, 2\pi)$, $\varphi \in [0, \pi]$) with respect to its center $\mathbf{c} \in \mathbb{R}^3$. Here, $\left(r_{\mathsf{xc}}, \theta_{\mathsf{xc}}, \varphi_{\mathsf{xc}}\right)^\top$ are coordinates of the vector $\mathbf{x}_{\mathbf{c}} := \mathbf{x} - \mathbf{c}$.

The radial dependence $\mathsf{f}\left(r_{\mathsf{xc}}\right)$ includes a singularity at the center, $\left|\mathsf{f}\left(r\right)\right| \to \infty$ for $r \to 0$, and the desired decay condition at infinity. Because of the singularity, multipoles must always be centered outside of the domain where they are used as a tool for approximation.

The spherical dependence $\mathbf{g}\left(\theta_{\mathsf{xc}}, \varphi_{\mathsf{xc}}\right)$ is generally formulated in terms of vector spherical harmonics [7, p. 289]. Additional constraints to the basis functions, like the Coulomb gauge in (1), are embedded in the vector spherical harmonics that express $\mathbf{g}$.

Specific multipoles chosen for our numerical experiments of Section 4 are:

$$
\mathbf{v}_{lm}\left(r_{xc}, \theta_{xc}, \varphi_{xc}\right) \;=\; -\frac{1}{l(2l+1)}\frac{1}{r_{xc}^{l+1}}\Phi_{lm}\left(\theta_{xc}, \varphi_{xc}\right), \quad l = 1,\ldots,\infty, \quad m = -l,\ldots,l,
$$
$$
\Phi_{lm}\left(\theta, \varphi\right) \;:=\; \mathbf{r}\times\nabla_{sph}Y_{lm}\left(\theta, \varphi\right), \quad \mathbf{r} = (r, 0, 0)^{\top},
\tag{4}
$$

where ∇_{sph} indicates the gradient in spherical coordinates and $Y_{lm}\left(\theta, \varphi\right)$ the spherical harmonics [1, p. 108–109]. It can be shown that $\Phi_{lm}\left(\theta, \varphi\right)$ does not depend on r despite the presence of $\mathbf{r}$ in its expression. These multipoles satisfy the decay condition (1b).

Each multipole is characterized by a location, i.e. its center $\mathbf{c}$, and the parameters l (degree) and m. In our convergence tests we always place several multipoles at a given location up to a certain order, which is the maximum degree of multipoles with that center. Hence, we use the term *multipole expansion* when referring to several multipoles in one point up to a certain order, which is the degree where the expansion is truncated.

3 | COUPLING STRATEGIES

We consider the partition $\mathbb{R}^3 = \Omega_f \cup \Gamma \cup \Omega_m$, $\Gamma := \partial\Omega_f = \partial\Omega_m$, $\Omega_f \cap \Omega_m = \varnothing$. Ω_f is a bounded Lipschitz domain, the FEM domain, whereas Ω_m is dubbed the MMP domain. The terminology indicates the type of approximation of $\mathbf{u}$ to be employed in each subdomain. Coupling is done across the interface Γ. We demand $\Omega_\star \subset \Omega_f$, but not necessarily $\Omega_\star = \Omega_f$. If $\Omega_\star \neq \Omega_f$, Γ is an artificial interface.

We define

$$
\mathbf{u}^f := \mathbf{u}|_{\Omega_f} \in \mathbf{H}\left(\mathbf{curl}, \Omega_f\right), \quad \mathbf{u}^m := \mathbf{u}|_{\Omega_m} \in \mathbf{H}_{loc}\left(\mathbf{curl}, \Omega_m\right),
\tag{5a}
$$

and

$$
\phi^f := \phi|_{\Omega_f} \in H^1_*\left(\Omega_f\right), \quad \phi^m := \phi|_{\Omega_m} = 0,
\tag{5b}
$$

as the divergence-free condition is already imposed strongly for functions $\mathbf{u}^m \in \mathcal{T}\left(\Omega_m\right)$. $H^1_*\left(\Omega_f\right)$ is defined as $\left\{v \in H^1\left(\Omega_f\right):\ \int_{\Omega_f} v\, d\mathbf{x} = 0\right\}$.

We denote by γ_m the *magnetic trace operator*:

$$
\gamma_m : \mathbf{H}_{loc}\left(\nabla\times\nabla, \Omega_\circ\right) \to \mathbf{H}^{-\frac{1}{2}}\left(\Gamma\right), \quad \gamma_m\mathbf{v} := \mathbf{n}\times\mathbf{M}\,\nabla\times\mathbf{v}, \quad \mathbf{v} \in \mathbf{H}_{loc}\left(\nabla\times\nabla, \Omega_\circ\right).
\tag{6}
$$

- $\mathbf{H}_{loc}\left(\nabla\times\nabla, \Omega_\circ\right)$ is the space of functions $\mathbf{v} \in \mathbf{H}_{loc}\left(\mathbf{curl}, \Omega_\circ\right)$ for which $\nabla\times\nabla\,\mathbf{v} \in \mathbf{L}^2_{loc}\left(\Omega_\circ\right)$, given $\circ = f, m$.

- We always take $\mathbf{n}$ as the normal pointing outwards with respect to Ω_f into Ω_m.

Across Γ the solution $\mathbf{u}$ of (1) has to satisfy the *transmission conditions* [8, p. 107, Lemma 5.3]

$$
\mathbf{n}\times\mathbf{u}^f|_\Gamma = \mathbf{n}\times\mathbf{u}^m|_\Gamma,
\tag{7a}
$$
$$
\gamma_m\mathbf{u}^f|_\Gamma = \gamma_m\mathbf{u}^m|_\Gamma,
\tag{7b}
$$
$$
\mathbf{n}\cdot\mathbf{u}^f|_\Gamma = \mathbf{n}\cdot\mathbf{u}^m|_\Gamma.
\tag{7c}
$$

(7a) and (7b) stem from the first line (Ampère's law) of the system (1a), (7c) from the second line (Coulomb gauge).

The starting point of all coupling approaches is the weak form of (1) in Ω_f. By testing the first PDE with $\mathbf{v}^f \in \mathbf{H}\left(\mathbf{curl}, \Omega_f\right)$ and the second with $\psi^f \in H^1_*\left(\Omega_f\right)$, integrating by parts over Ω_f, and using the transmission conditions (7b) and (7c), we obtain

$$
\begin{cases}
\int_{\Omega_f}\left(\mathbf{M}\,\nabla\times\mathbf{u}^f\right)\cdot\left(\nabla\times\mathbf{v}^f\right)\,d\mathbf{x} + \int_\Gamma \gamma_m\mathbf{u}^m\cdot\mathbf{v}^f\,dS + \int_{\Omega_f}\nabla\phi^f\cdot\mathbf{v}^f\,d\mathbf{x} = \int_{\Omega_f}\mathbf{f}\cdot\mathbf{v}^f\,d\mathbf{x} & \forall\mathbf{v}^f \in \mathbf{H}\left(\mathbf{curl}, \Omega_f\right) \\
\int_{\Omega_f}\mathbf{u}^f\cdot\nabla\psi^f\,d\mathbf{x} - \int_\Gamma \left(\mathbf{n}\cdot\mathbf{u}^m\right)\psi^f\,dS = 0 & \forall\psi^f \in H^1_*\left(\Omega_f\right)
\end{cases}
\tag{8}
$$

We end up with different coupling approaches depending on how we impose the additional transmission condition (7a). Each coupling approach can be expressed as a minimization problem for different *Lagrangian functionals*, to be discussed in the following sections. The resulting *linear variational saddle point problems* will also be illustrated. Exception to this scheme is the approach described in Section 3.4, where a Lagrangian formulation is not possible.

Discretization

Throughout we use tetrahedral meshes $\mathcal{M}_f$ on Ω_f. We discretize $\mathbf{u}^f \in \mathbf{H}\left(\mathbf{curl}, \Omega_f\right)$ with the lowest-order $\mathbf{H}\left(\mathbf{curl}, \Omega_f\right)$-conforming edge elements of the first family due to Nédélec [9], i.e.

$$
\mathbf{V}_n\left(\mathcal{M}_f\right) := \left\{\mathbf{v}_n \in \mathbf{H}_0\left(\mathbf{curl}, \Omega_f\right):\ \mathbf{v}_n|_K\left(\mathbf{x}\right) = \mathbf{a}_K + \mathbf{b}_K\times\mathbf{x}, \quad \mathbf{a}_K, \mathbf{b}_K \in \mathbb{R}^3, \ \mathbf{x} \in K \quad \forall K \in \mathcal{M}_f\right\},
\tag{9a}
$$

and $\phi^f \in H^1_* (\Omega_f)$ with piecewise linear Lagrangian finite elements, i.e.

$$V_n (\mathcal{M}_f) := \left\{ v_n \in C^0 (\Omega_f) : \ v_n|_K (\mathbf{x}) = a_K + \mathbf{b}_K \cdot \mathbf{x}, \quad a_K \in \mathbb{R}, \ \mathbf{b}_K \in \mathbb{R}^3, \ \mathbf{x} \in K \quad \forall K \in \mathcal{M}_f \right\}. \tag{9b}$$

On discrete functions $\phi^f_n \in V_n (\mathcal{M}_f) \subset H^1 (\Omega_f)$ we impose the condition $\int_{\Omega_f} \phi^f_n \, d\mathbf{x} = 0$ by means of a scalar Lagrange multiplier.

For Ω_m we take some multipoles to form the discrete space $\mathcal{T}_n (\Omega_m) \subset \mathcal{T} (\Omega_m)$. The size of $\mathcal{T}_n (\Omega_m)$ is determined by the number of multipole expansions chosen for the approximation and their orders.

3.1 | PDE-constrained Least-Squares Coupling

Taking the cue from (7a), we seek $\mathbf{u}^f \in \mathbf{H} (\mathbf{curl}, \Omega_f)$, $\mathbf{u}^m \in \mathcal{T} (\Omega_m)$,

- minimizing

$$J_\Gamma \left(\mathbf{u}^f, \mathbf{u}^m \right) := \| \mathbf{n} \times \mathbf{u}^f - \mathbf{n} \times \mathbf{u}^m \|^2_{\mathbf{H}^{-\frac{1}{2}} (\mathrm{div}_\Gamma, \Gamma)} \tag{10}$$

- and satisfying the constraint (8).

These two conditions determine a quadratic minimization problem under a linear variational constraint where we switch the usual meaning of these two components: here the constraint is given by the variational form of the minimization problem that satisfies the system of PDEs (8) in Ω_f, while the functional J_Γ to be minimized is the additional transmission condition not imposed by the variational form.

This problem can be rephrased as seeking a saddle point of the following Lagrangian:

$$\begin{aligned} L \left(\mathbf{u}^f, \mathbf{u}^m, \phi^f, \mathbf{p}^f, \xi^f \right) := & \ \tfrac{1}{2} \| \mathbf{n} \times \mathbf{u}^f - \mathbf{n} \times \mathbf{u}^m \|^2_{\mathbf{H}^{-\frac{1}{2}} (\mathrm{div}_\Gamma, \Gamma)} + \\ & \int_{\Omega_f} \left(\mathbf{M} \, \nabla \times \mathbf{u}^f \right) \cdot \left(\nabla \times \mathbf{p}^f \right) \, d\mathbf{x} + \int_\Gamma \gamma_m \mathbf{u}^m \cdot \mathbf{p}^f \, dS + \int_{\Omega_f} \nabla \phi^f \cdot \mathbf{p}^f \, d\mathbf{x} - \int_{\Omega_f} \mathbf{f} \cdot \mathbf{p}^f + \\ & \int_{\Omega_f} \mathbf{u}^f \cdot \nabla \xi^f \, d\mathbf{x} - \int_\Gamma (\mathbf{n} \cdot \mathbf{u}^m) \, \xi^f \, dS. \end{aligned} \tag{11}$$

- $\phi^f \in H^1_* (\Omega_f)$, as discussed in Section 3.

- $\mathbf{p}^f \in \mathbf{H} (\mathbf{curl}, \Omega_f)$ is the Lagrange multiplier imposing the first line of (8).

- $\xi^f \in H^1_* (\Omega_f)$ is the Lagrange multiplier imposing the second line of (8).

For convenience we replace (10) with the $\mathbf{L}^2 (\Gamma)$-norm,

$$J_\Gamma \left(\mathbf{u}^f, \mathbf{u}^m \right) := \| \mathbf{n} \times \mathbf{u}^f - \mathbf{n} \times \mathbf{u}^m \|^2_{\mathbf{L}^2(\Gamma)}, \tag{12}$$

by seeking $\mathbf{u}^f \in \mathbf{H}_\Gamma (\mathbf{curl}, \Omega_f) := \left\{ \mathbf{v} \in \mathbf{H} (\mathbf{curl}, \Omega_f) : \ \mathbf{n} \times \mathbf{v}|_\Gamma \in \mathbf{L}^2_t (\Gamma) \right\}$.

The necessary and sufficient optimality conditions of (11) considering (12) give rise to the saddle point problem

$$\text{Seek } \mathbf{u}^f \in \mathbf{H}_\Gamma (\mathbf{curl}, \Omega_f), \ \mathbf{u}^m \in \mathcal{T} (\Omega_m), \ \phi^f \in H^1_* (\Omega_f), \ \mathbf{p}^f \in \mathbf{H} (\mathbf{curl}, \Omega_f), \ \xi^f \in H^1_* (\Omega_f):$$

$$\begin{cases} a^{LS} \left[\left(\mathbf{u}^f, \mathbf{u}^m \right), \left(\mathbf{v}^f, \mathbf{v}^m \right) \right] & + \ b^{LS} \left[\left(\mathbf{v}^f, \mathbf{v}^m, \psi^f \right), \left(\mathbf{p}^f, \xi^f \right) \right] \ = 0 \\ b^{LS} \left[\left(\mathbf{u}^f, \mathbf{u}^m, \phi^f \right), \left(\mathbf{q}^f, \zeta^f \right) \right] & = \int_{\Omega_f} \mathbf{f} \cdot \mathbf{q}^f \, d\mathbf{x} \end{cases} \tag{13}$$

$$\forall \mathbf{v}^f \in \mathbf{H}_\Gamma (\mathbf{curl}, \Omega_f), \ \forall \mathbf{v}^m \in \mathcal{T} (\Omega_m), \ \forall \psi^f \in H^1_* (\Omega_f), \ \forall \mathbf{q}^f \in \mathbf{H} (\mathbf{curl}, \Omega_f), \ \forall \zeta^f \in H^1_* (\Omega_f),$$

where

$$a^{LS} \left[\left(\mathbf{u}^f, \mathbf{u}^m \right), \left(\mathbf{v}^f, \mathbf{v}^m \right) \right] := \int_\Gamma \left[\mathbf{n} \times \left(\mathbf{u}^f - \mathbf{u}^m \right) \right] \cdot \left[\mathbf{n} \times \left(\mathbf{v}^f - \mathbf{v}^m \right) \right] \, dS, \tag{14a}$$

$$b^{LS} \left[\left(\mathbf{u}^f, \mathbf{u}^m, \phi^f \right), \left(\mathbf{q}^f, \zeta^f \right) \right] := \int_{\Omega_f} \left(\mathbf{M} \, \nabla \times \mathbf{u}^f \right) \cdot \left(\nabla \times \mathbf{q}^f \right) \, d\mathbf{x} + \int_\Gamma \gamma_m \mathbf{u}^m \cdot \mathbf{q}^f \, dS + \int_{\Omega_f} \nabla \phi^f \cdot \mathbf{q}^f + \int_{\Omega_f} \mathbf{u}^f \cdot \nabla \zeta^f \, d\mathbf{x} - \int_\Gamma (\mathbf{n} \cdot \mathbf{u}^m) \, \zeta^f \, dS. \tag{14b}$$

We propose the following discretization for (13):

- $\mathbf{u}^f, \mathbf{v}^f, \mathbf{p}^f, \mathbf{q}^f \in \mathbf{V}_n (\mathcal{M}_f)$ of (9a),

- $\phi^f, \psi^f, \xi^f, \zeta^f \ \in V_n (\mathcal{M}_f)$ of (9b), and

- $\mathbf{u}^m, \mathbf{v}^m \in \mathcal{T}_n (\Omega_m)$.

3.2 | Multi-Field Coupling

The *multi-field domain decomposition method* allows to use FEM with nonconforming meshes on different domains for the same boundary value problem [10]. This is well-suited for the coupling because one can think of MMP as FEM with special functions acting on a "mesh of a single entity" defined on Ω_m.

For Maxwell's equations, the multi-field method imposes tangential continuity in a weak sense by means of a Lagrange multiplier $\boldsymbol{\lambda} := \boldsymbol{\gamma}_m \mathbf{u}^m$. However, given the defining equation of $\boldsymbol{\lambda}$ and the generalized Stokes' theorem in $\mathbf{H}\left(\mathbf{curl}, \Omega\right)$ [8, p. 59, Theorem 3.31], what is actually imposed is the continuity of the *tangential components trace*,

$$\mathbf{n} \times \left(\mathbf{n} \times \mathbf{u}^f\right)\big|_\Gamma = \mathbf{n} \times \left(\mathbf{n} \times \mathbf{u}^m\right)\big|_\Gamma \,, \tag{15}$$

instead of the continuity between *twisted tangential traces* implied by (7a). Note that (15) is an equation connecting traces in $\mathbf{H}^{-\frac{1}{2}}\left(\mathrm{curl}_\Gamma, \Gamma\right)$ and therefore it has to be tested with functions in the dual space $\mathbf{H}^{-\frac{1}{2}}\left(\mathrm{div}_\Gamma, \Gamma\right)$.

Hence, the multi-field coupling can be expressed by the following Lagrangian:

$$\mathrm{L}\left(\mathbf{u}^f, \mathbf{u}^m, \phi^f, \boldsymbol{\lambda}\right) := \mathrm{J}_{\Omega_f}\left(\mathbf{u}^f, \phi^f\right) + \mathrm{J}_{\Omega_m}\left(\mathbf{u}^m\right) + \int_\Gamma \left\{\mathbf{n} \times \left[\mathbf{n} \times \left(\mathbf{u}^f - \mathbf{u}^m\right)\right]\right\} \cdot \boldsymbol{\lambda} \,\mathrm{dS} \,. \tag{16}$$

The functional J_{Ω_f} expresses the saddle point problem that satisfies (1a) for $\mathbf{u}^f$ in Ω_f:

$$\mathrm{J}_{\Omega_f}\left(\mathbf{u}^f, \phi^f\right) := \frac{1}{2}\int_{\Omega_f} \left(\mathbf{M} \nabla \times \mathbf{u}^f\right) \cdot \left(\nabla \times \mathbf{u}^f\right) \,\mathrm{d}\mathbf{x} - \int_{\Omega_f} \mathbf{f} \cdot \mathbf{u}^f \,\mathrm{d}\mathbf{x} + \int_{\Omega_f} \mathbf{u}^f \cdot \nabla \phi^f \,\mathrm{d}\mathbf{x} - \int_\Gamma \left(\mathbf{n} \cdot \mathbf{u}^f\right) \phi^f \,\mathrm{dS} \,. \tag{17a}$$

The functional J_{Ω_m} for $\mathbf{u}^m$ in Ω_m has a similar formulation, but for a homogeneous problem:

$$\mathrm{J}_{\Omega_m}\left(\mathbf{u}^m\right) := \frac{1}{2}\int_{\Omega_m} \|\nabla \times \mathbf{u}^m\|_{\ell^2}^2 = \frac{1}{2}\int_\Gamma \boldsymbol{\gamma}_m \mathbf{u}^m \cdot \mathbf{u}^m \,\mathrm{dS} \,. \tag{17b}$$

A Lagrange multiplier ϕ to impose the divergence-free condition is not required given $\mathbf{u}^m \in \boldsymbol{\mathcal{T}}\left(\Omega_m\right)$: see (5b).

We therefore obtain the following saddle point problem:

$$\text{Seek } \mathbf{u}^f \in \mathbf{H}\left(\mathbf{curl}, \Omega_f\right), \, \mathbf{u}^m \in \boldsymbol{\mathcal{T}}\left(\Omega_m\right), \, \phi^f \in \mathrm{H}_*^1\left(\Omega_f\right), \, \boldsymbol{\lambda} \in \mathbf{H}^{-\frac{1}{2}}\left(\mathrm{div}_\Gamma, \Gamma\right):$$

$$\begin{cases} \mathrm{a}^{\mathsf{MF}}\left[\left(\mathbf{u}^f, \mathbf{u}^m\right), \left(\mathbf{v}^f, \mathbf{v}^m\right)\right] \;+\; \mathrm{b}^{\mathsf{MF}}\left[\left(\mathbf{v}^f, \mathbf{v}^m\right), \left(\phi^f, \boldsymbol{\lambda}\right)\right] \;=\; \int_{\Omega_f} \mathbf{f} \cdot \mathbf{v}^f \,\mathrm{d}\mathbf{x} \\ \mathrm{b}^{\mathsf{MF}}\left[\left(\mathbf{u}^f, \mathbf{u}^m\right), \left(\psi^f, \boldsymbol{\chi}\right)\right] \hspace{4.5cm} =\; 0 \end{cases} \tag{18}$$

$$\forall \mathbf{v}^f \in \mathbf{H}\left(\mathbf{curl}, \Omega_f\right), \, \forall \mathbf{v}^m \in \boldsymbol{\mathcal{T}}\left(\Omega_m\right), \, \forall \psi^f \in \mathrm{H}_*^1\left(\Omega_f\right), \, \boldsymbol{\chi} \in \mathbf{H}^{-\frac{1}{2}}\left(\mathrm{div}_\Gamma, \Gamma\right),$$

where

$$\mathrm{a}^{\mathsf{MF}}\left[\left(\mathbf{u}^f, \mathbf{u}^m\right), \left(\mathbf{v}^f, \mathbf{v}^m\right)\right] := \int_{\Omega_f} \left(\mathbf{M} \nabla \times \mathbf{u}^f\right) \cdot \left(\nabla \times \mathbf{v}^f\right) \,\mathrm{d}\mathbf{x} + \int_\Gamma \boldsymbol{\gamma}_m \mathbf{u}^m \cdot \mathbf{v}^m \,\mathrm{dS} \,, \tag{19a}$$

$$\mathrm{b}^{\mathsf{MF}}\left[\left(\mathbf{u}^f, \mathbf{u}^m\right), \left(\psi^f, \boldsymbol{\chi}\right)\right] := \int_{\Omega_f} \mathbf{u}^f \cdot \nabla \psi^f \,\mathrm{d}\mathbf{x} - \int_\Gamma \left(\mathbf{n} \cdot \mathbf{u}^m\right) \psi^f \,\mathrm{dS} + \int_\Gamma \left\{\mathbf{n} \times \left[\mathbf{n} \times \left(\mathbf{u}^f - \mathbf{u}^m\right)\right]\right\} \cdot \boldsymbol{\chi} \,\mathrm{dS} \,. \tag{19b}$$

We inserted (7c) into (17a) to define $\mathrm{b}^{\mathsf{MF}}\left(\cdot, \cdot\right)$.

For the discretization of (18), we suggest $\mathbf{u}^f, \mathbf{v}^f \in \mathbf{V}_n\left(\mathcal{M}_f\right)$ of (9a), $\phi^f, \psi^f \in \mathrm{V}_n\left(\mathcal{M}_f\right)$ of (9b), and $\mathbf{u}^m, \mathbf{v}^m \in \boldsymbol{\mathcal{T}}_n\left(\Omega_m\right)$.

The discretization of $\boldsymbol{\lambda} \in \mathbf{H}^{-\frac{1}{2}}\left(\mathrm{div}_\Gamma, \Gamma\right)$ is a topic debated in the literature [11, Section 4]. We opted for the trace on Γ of the elements of the Nédélec's space $\mathbf{V}_n$. Note that we ignore the duality of $\boldsymbol{\lambda}$, choosing a nonconforming $\boldsymbol{\lambda}_n \notin \mathbf{H}^{-\frac{1}{2}}\left(\mathrm{div}_\Gamma, \Gamma\right)$, which represents the most common discretization strategy [11, Section 4.1].

3.3 | Discontinuous Galerkin

As for the multi-field coupling (Section 3.2), we again treat MMP as an element of FEM. Here we exploit the other main approach for imposing weak continuity on non-conforming meshes, which is *Discontinuous Galerkin*. Specifically, we want to impose weak continuity of the tangential components (7a) [12].

Under this idea, the coupling can be expressed as a *discrete* minimization problem for the following Lagrangian:

$$\mathrm{L}\left(\mathbf{u}_n^f, \mathbf{u}_n^m, \phi_n^f\right) := \mathrm{J}_{\Omega_f}\left(\mathbf{u}_n^f, \phi_n^f\right) + \mathrm{J}_{\Omega_m}\left(\mathbf{u}_n^m\right) + \int_\Gamma \left[\mathbf{n} \times \left(\mathbf{u}_n^f - \mathbf{u}_n^m\right)\right] \cdot \mathbf{P}_n \left[\mathbf{n} \times \left(\mathbf{u}_n^f - \mathbf{u}_n^m\right)\right] \,\mathrm{dS} \,, \tag{20}$$

where $\mathbf{u}_n^f \in \mathbf{V}_n\left(\mathcal{M}_f\right)$ of (9a), $\phi_n^f \in \mathrm{V}_n\left(\mathcal{M}_f\right)$ of (9b), and $\mathbf{u}_n^m \in \boldsymbol{\mathcal{T}}_n\left(\Omega_m\right)$. J_{Ω_f} and J_{Ω_m} are the same as in (17a) and (17b).

Depending on the choice of the discrete operator $\mathbf{P_n} : \mathbf{H}^{\frac{1}{2}}(\Gamma) \to \mathbf{H}^{-\frac{1}{2}}(\Gamma)$, we obtain different DG approaches. We follow the *Interior Penalty DG method* [13]:

$$\mathbf{P_n}(\mathbf{u}) := -\epsilon_\mathbf{n} \, \overline{\mathbf{M}} \, \nabla \times \mathbf{u} + \frac{\eta}{\mathsf{h}} \, \overline{\mathbf{M}} \, \mathbf{u} \,. \tag{21}$$

- $\epsilon_\mathbf{n}(\mathbf{x}) : \mathbb{R}^3 \to \mathbb{R}$ is $= +1$ if you are integrating on an intersection of the FEM mesh $\mathcal{M_f}$ on Γ from the side of Ω_f and $= -1$ if you are integrating from the side of Ω_m.

- $\overline{\mathbf{M}}(\mathbf{x}) : \mathbb{R}^3 \to \mathbb{R}^3$ is the mean of the material parameters of Ω_f and Ω_m on Γ:

$$\overline{\mathbf{M}}(\mathbf{x}) := \frac{\mathbf{M}(\mathbf{x}) + \mathbf{I}}{2} \quad \forall \mathbf{x} \in \Gamma \,. \tag{22}$$

- $\eta \in \mathbb{R}$ is a penalty parameter that needs to be set heuristically. It should depend on the number of degrees of freedom of MMP.

- $\mathsf{h} \in \mathbb{R}$ is the diameter of the intersection of $\mathcal{M_f}$ on Γ where you are integrating.

Finding the stationary point of (20) leads to the discrete saddle point problem

$$\text{Seek } \mathbf{u_n^f} \in \mathbf{V_n} \subset \mathbf{H}(\mathbf{curl}, \Omega_\mathsf{f}), \, \mathbf{u_n^m} \in \boldsymbol{\mathcal{T}_n} \subset \boldsymbol{\mathcal{T}}(\Omega_\mathsf{m}), \, \phi_\mathsf{n}^\mathsf{f} \in \mathsf{V_n} \subset \mathsf{H}_*^1(\Omega_\mathsf{f}) :$$

$$\begin{cases} \mathrm{a_n^{DG}}\left[\left(\mathbf{u_n^f}, \mathbf{u_n^m}\right), \left(\mathbf{v_n^f}, \mathbf{v_n^m}\right)\right] \, + \, \mathrm{b_n^{DG}}\left[\left(\mathbf{v_n^f}, \mathbf{v_n^m}\right), \phi_\mathsf{n}^\mathsf{f}\right] \, = \int_{\Omega_\mathsf{f}} \mathbf{f} \cdot \mathbf{v_n^f} \, \mathrm{d}\mathbf{x} \\ \mathrm{b_n^{DG}}\left[\left(\mathbf{u_n^f}, \mathbf{u_n^m}\right), \psi_\mathsf{n}^\mathsf{f}\right] \qquad\qquad\qquad\qquad\quad = 0 \end{cases} \tag{23}$$

$$\forall \mathbf{v_n^f} \in \mathbf{V_n} \subset \mathbf{H}(\mathbf{curl}, \Omega_\mathsf{f}), \, \forall \mathbf{v_n^m} \in \boldsymbol{\mathcal{T}_n} \subset \boldsymbol{\mathcal{T}}(\Omega_\mathsf{m}), \, \forall \psi_\mathsf{n}^\mathsf{f} \in \mathsf{V_n} \subset \mathsf{H}_*^1(\Omega_\mathsf{f}) \,.$$

As usual, we define a symmetric bilinear form $\mathrm{a_n^{DG}}(\cdot, \cdot)$ and linear form $\mathrm{b_n^{DG}}(\cdot, \cdot)$:

$$\mathrm{a_n^{DG}}\left[\left(\mathbf{u_n^f}, \mathbf{u_n^m}\right), \left(\mathbf{v_n^f}, \mathbf{v_n^m}\right)\right] := \int_{\Omega_\mathsf{f}} \left(\mathbf{M} \, \nabla \times \mathbf{u_n^f}\right) \cdot \left(\nabla \times \mathbf{v_n^f}\right) \, \mathrm{d}\mathbf{x} + \int_\Gamma \boldsymbol{\gamma}_\mathsf{m} \mathbf{u_n^m} \cdot \mathbf{v_n^m} \, \mathrm{dS} - \tag{24a}$$

$$\int_\Gamma \left[\overline{\mathbf{M}} \, \nabla \times \left(\mathbf{u_n^f} + \mathbf{u_n^m}\right)\right] \cdot \left[\mathbf{n} \times \left(\mathbf{v_n^f} - \mathbf{v_n^m}\right)\right] \, \mathrm{dS} - \int_\Gamma \left[\mathbf{n} \times \left(\mathbf{u_n^f} - \mathbf{u_n^m}\right)\right] \cdot \left[\overline{\mathbf{M}} \, \nabla \times \left(\mathbf{v_n^f} + \mathbf{v_n^m}\right)\right] \, \mathrm{dS} +$$

$$\int_\Gamma \frac{2\,\eta}{\mathsf{h}} \left[\overline{\mathbf{M}} \, \mathbf{n} \times \left(\mathbf{u_n^f} - \mathbf{u_n^m}\right)\right] \cdot \left[\mathbf{n} \times \left(\mathbf{v_n^f} - \mathbf{v_n^m}\right)\right] \, \mathrm{dS} \,,$$

$$\mathrm{b_n^{DG}}\left[\left(\mathbf{u_n^f}, \mathbf{u_n^m}\right), \psi_\mathsf{n}^\mathsf{f}\right] := \int_{\Omega_\mathsf{f}} \mathbf{u^f} \cdot \nabla \psi^\mathsf{f} \, \mathrm{d}\mathbf{x} - \int_\Gamma (\mathbf{n} \cdot \mathbf{u^m}) \, \psi^\mathsf{f} \, \mathrm{dS} \,. \tag{24b}$$

We inserted (7c) into (17a) to define $\mathrm{b_n^{DG}}(\cdot, \cdot)$.

3.4 | Coupling by Tangential Traces

Instead of the continuity between twisted tangential traces implied by (7a), we take into account the continuity of the tangential components trace (15), as in Section 3.2. (15) is imposed in weak form by testing it with $\mathbf{v^m} \in \boldsymbol{\mathcal{T}}(\Omega_\mathsf{m})$:

$$\int_\Gamma \left[\mathbf{n} \times \left(\mathbf{n} \times \mathbf{u^f}\right)\right] \cdot \mathbf{v^m} \, \mathrm{d}S - \int_\Gamma \left[\mathbf{n} \times \left(\mathbf{n} \times \mathbf{u^m}\right)\right] \cdot \mathbf{v^m} \, \mathrm{d}S = 0 \qquad \forall \mathbf{v^m} \in \boldsymbol{\mathcal{T}}(\Omega_\mathsf{m}) \,. \tag{25}$$

Combining (25) with the variational form of (8), we end up with the following system:

$$\text{Seek } \mathbf{u_n^f} \in \mathbf{V_n} \subset \mathbf{H}(\mathbf{curl}, \Omega_\mathsf{f}), \, \mathbf{u_n^m} \in \boldsymbol{\mathcal{T}_n} \subset \boldsymbol{\mathcal{T}}(\Omega_\mathsf{m}), \, \phi_\mathsf{n}^\mathsf{f} \in \mathsf{V_n} \subset \mathsf{H}_*^1(\Omega_\mathsf{f}) :$$

$$\begin{cases} \int_{\Omega_\mathsf{f}} \left(\mathbf{M} \, \nabla \times \mathbf{u^f}\right) \cdot \left(\nabla \times \mathbf{v^f}\right) \, \mathrm{d}\mathbf{x} + \int_\Gamma \boldsymbol{\gamma}_\mathsf{m} \mathbf{u^m} \cdot \mathbf{v^f} \, \mathrm{dS} + \int_{\Omega_\mathsf{f}} \nabla \phi^\mathsf{f} \cdot \mathbf{v^f} \, \mathrm{d}\mathbf{x} = \int_{\Omega_\mathsf{f}} \mathbf{f} \cdot \mathbf{v^f} \, \mathrm{d}\mathbf{x} \\ \int_\Gamma \left[\mathbf{n} \times \left(\mathbf{n} \times \mathbf{u^f}\right)\right] \cdot \mathbf{v^m} \, \mathrm{dS} - \int_\Gamma \left[\mathbf{n} \times \left(\mathbf{n} \times \mathbf{u^m}\right)\right] \cdot \mathbf{v^m} \, \mathrm{dS} = 0 \\ \int_{\Omega_\mathsf{f}} \mathbf{u^f} \cdot \nabla \psi^\mathsf{f} \, \mathrm{d}\mathbf{x} - \int_\Gamma (\mathbf{n} \cdot \mathbf{u^m}) \, \psi^\mathsf{f} \, \mathrm{dS} = 0 \end{cases} \tag{26}$$

$$\forall \mathbf{v_n^f} \in \mathbf{V_n} \subset \mathbf{H}(\mathbf{curl}, \Omega_\mathsf{f}), \, \forall \mathbf{v_n^m} \in \boldsymbol{\mathcal{T}_n} \subset \boldsymbol{\mathcal{T}}(\Omega_\mathsf{m}), \, \forall \psi_\mathsf{n}^\mathsf{f} \in \mathsf{V_n} \subset \mathsf{H}_*^1(\Omega_\mathsf{f}) \,.$$

Galerkin discretization of (26) is straightforward: as in Section 3.3, we replace $\mathbf{H}(\mathbf{curl}, \Omega_\mathsf{f})$ with the Nédélec's finite element space $\mathbf{V_n}(\mathcal{M_f})$ of (9a), $\mathsf{H}^1(\Omega_\mathsf{f})$ with the Lagrangian finite element space $\mathsf{V_n}(\mathcal{M_f})$ of (9b), and $\boldsymbol{\mathcal{T}}(\Omega_\mathsf{m})$ with a finite-dimensional subspace $\boldsymbol{\mathcal{T}}_\mathsf{n}(\Omega_\mathsf{m})$.
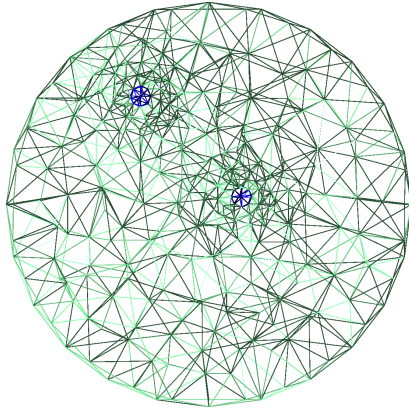
FIGURE 1 Cross-section of the 3D mesh of the FEM domain Ω_f along the YZ-plane. The blue mesh represents $\Omega_\star$. The green mesh is a hollow ball centered in the origin that, in the mesh shown, has radius 2.

4 | NUMERICAL EXPERIMENTS

To study the convergence we employ uniform h-refinement of $\mathcal{M}_f$ and p-refinement of the Trefftz approximation, in the sense that we increase the number of multipole expansions. We monitor the following $\mathbf{L}^2$-errors:

- The error in the FEM domain, which is the relative $\mathbf{L}^2(\Omega_f)$-error compared to the reference solution in Ω_f, i.e.

$$\left\| \mathbf{u} - \sum_{i=1}^{n} \alpha_i \, \mathbf{v}_i(\mathbf{x}) \right\|_{\mathbf{L}^2(\Omega_f)} \Bigg/ \|\mathbf{u}\|_{\mathbf{L}^2(\Omega_f)}, \quad \alpha_i \in \mathbb{R}, \; \mathbf{v}_i \in \mathbf{V}_n(\mathcal{M}_f), \quad i = 1, \ldots, n. \tag{27}$$

- The MMP error on the interface, which is the relative $\mathbf{L}^2(\Gamma)$-error compared to the reference solution on Γ.

The sum of the relative $\mathbf{L}^2$-error for FEM in Ω_f and the relative $\mathbf{L}^2$-error for MMP on Γ is the total relative error of the coupling.

To ignore the impact of numerical integration for FEM, we use a Gaussian quadrature rule that is exact for polynomials of degree 2 (order 3).

Implementation

Meshes were generated using `COMSOL` [14] and `Gmsh` [15].

Our code is written in `C++14`, using `C++11` multithreading for parallelization. We use `Eigen` v3.3.4 [16] for linear algebra and `HyDi` [17] for the FEM component. The `PARDISO` v5.0.0 solver [18] provides the sparse LU decomposition to invert the matrices of the coupling, characterized by nontrivial sparsity patterns.

4.1 | Maxwell's Equations with Exact Solution

We solve $\nabla \times \nabla \times \mathbf{u} = \mathbf{j}$, $\nabla \cdot \mathbf{u} = 0$. $\Omega_\star$ is a loop of radius 0.1 centered at $(0, 0, 0.5)^\top$ and with normal axis $\left(0, \frac{\sqrt{2}}{2}, \frac{\sqrt{2}}{2}\right)^\top$. In $\Omega_\star$, $\|\mathbf{j}\| = 1.05 \cdot 10^6$ and is tangential to the loop; elsewhere, $\mathbf{j} = \mathbf{0}$. A sample mesh is shown in Figure 1.

We consider two different auxiliary boundaries Γ between Ω_f and Ω_m: two spheres centered in the origin of radius 4 and 2. Given that we use tetrahedral meshes, Γ is actually a polyhedral approximation of a sphere.

Multipole expansions are uniformly positioned on a circle of radius 1 centered in the origin and lying on the XY-plane. This positioning has been chosen to show that with auxiliary boundaries Γ one can properly approximate $\mathbf{u}$ in Ω_m regardless of the locations of the multipoles. We only use multipole expansions of order 1.

Figure 2 shows h-refinement convergence plots for the PDE-constrained coupling. We can clearly identify a linear convergence of the FEM error when Γ has radius 4, while the convergence is much slower with radius 2, when the multipoles are closer to the source of the field in $\Omega_\star$. In both cases, the MMP error decreases much more slowly. This is due to the fact that the exact solution is so easy to approximate in Ω_m that it can already be represented by very few multipoles. The number of multipoles is set to the natural logarithm of the number of vertices of the FEM meshes on the boundary Γ.

Plots obtained with the other approaches look the same as Figure 2.

Figure 3 shows surface plots of the total relative $\mathbf{L}^2$-error for the PDE-constrained coupling. The error is much lower for Γ of radius 4 than 2, decreases with h (algebraic convergence), and is generally independent from the number of multipoles. However, the error also becomes worse with the coarsest meshes and the highest numbers of multipoles considered, when the coupling is mostly difficult due to a disproportionately large number of degrees of freedom for MMP (dense blocks of the coupling matrices) with respect to FEM (sparse blocks). The MMP error dominates.
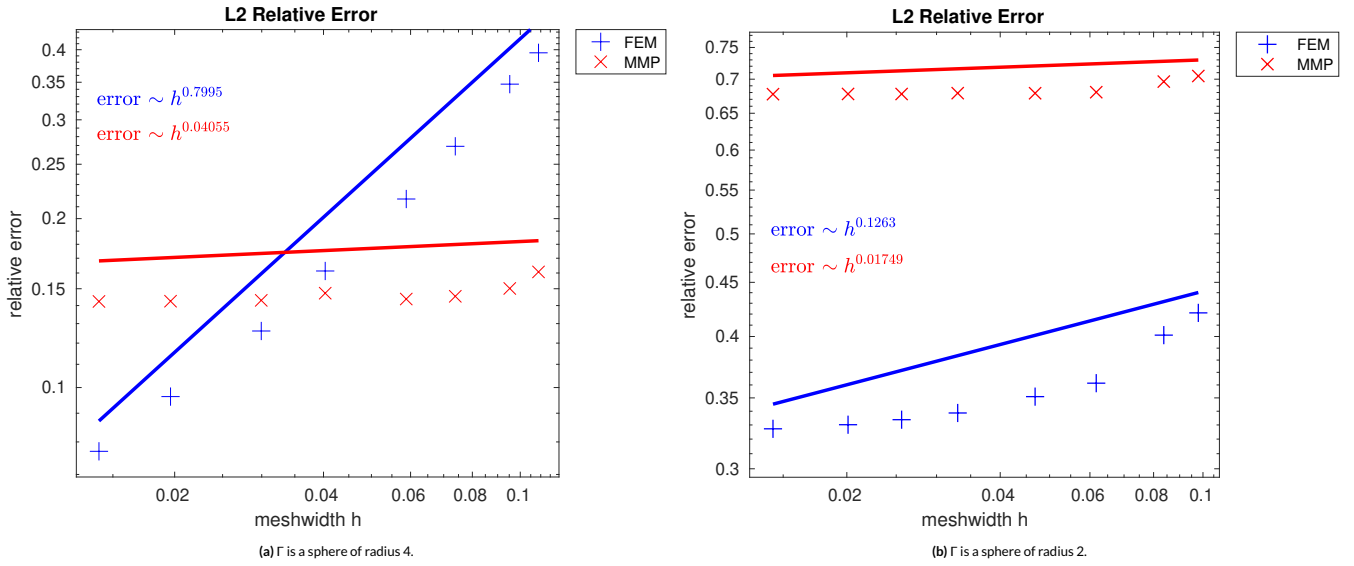
(a) Γ is a sphere of radius 4.

(b) Γ is a sphere of radius 2.

FIGURE 2 h-refinement plots for Maxwell's equations with exact solution. Plots obtained with the PDE-constrained coupling.

(a) Ω_f is a sphere of radius 4.
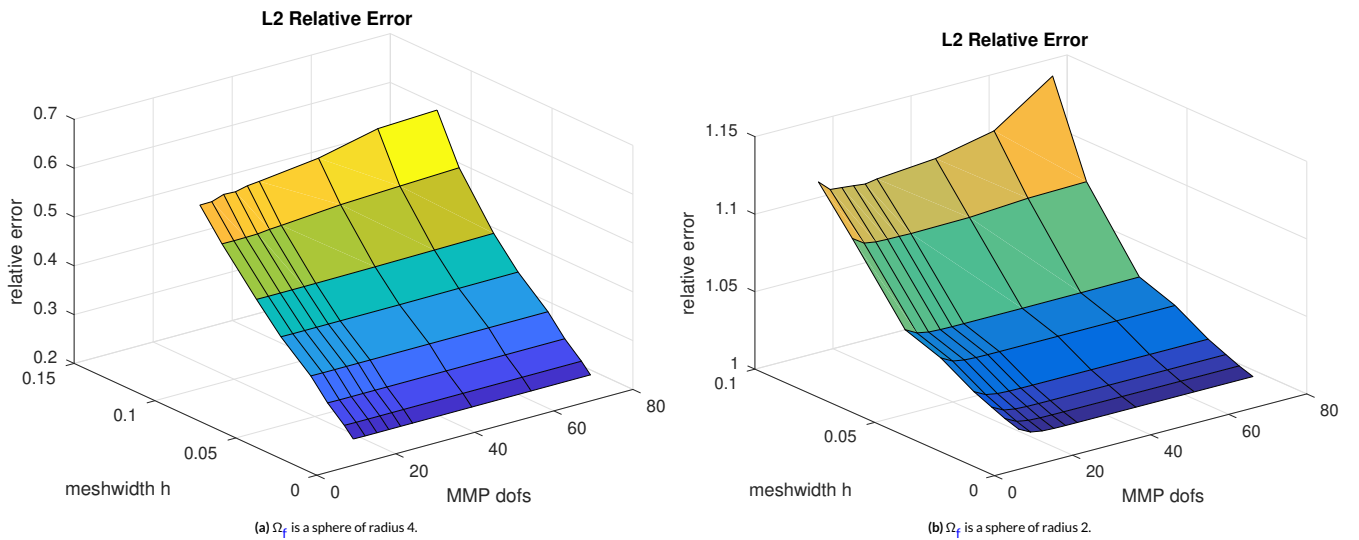
(b) Ω_f is a sphere of radius 2.

FIGURE 3 Meshwidth h vs. MMP degrees of freedom for Maxwell's equations with exact solution: total relative error. Plots obtained with the PDE-constrained coupling.

Plots obtained with the other approaches look the same as Figure 3, except for even larger errors with the coarsest meshes and highest numbers of multipoles considered.
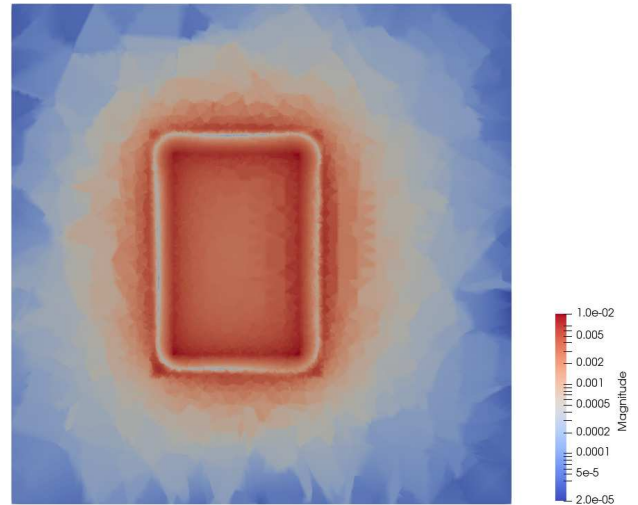
4.2 | Magnetostatic Inductor

We solve $\nabla \times (\kappa \nabla \times \mathbf{u}) = \mathbf{j}$, $\nabla \cdot \mathbf{u} = 0$. $\Omega_\star$ is composed of three regions: two hollow cylinders and one hollow rectangular prism. In the cylinders, $\mathbf{j}$ is tangential to the lateral surfaces, with opposite directions and $\|\mathbf{j}\| = 1.05 \cdot 10^6$ or $= 1.25 \cdot 10^6$ in each of the cylinders. In the prism, $\kappa \sim \nabla \times \mathbf{u}$ according to a given curve (*hysteresis loop*). Elsewhere, $\mathbf{j} = \mathbf{0}$ and $\kappa = 1$. The mesh is shown in Figure 4a.

Multipole expansions are positioned in the centers of the entities of a very coarse surface mesh (24 triangles) on a rectangular prism with sizes $0.15 \times 0.15 \times 0.1$. We only use multipole expansions of order 1.

Figure 4b shows a plot of the magnitude of the numerical solution $\|\mathbf{u}_n\|$ for the multi-field coupling. A plot obtained with the PDE-constrained coupling looks the same. Results were collected after 10 iterations to let $\kappa \sim \nabla \times \mathbf{u}$ converge to a stable value for each entity of $\mathcal{M}_f$.
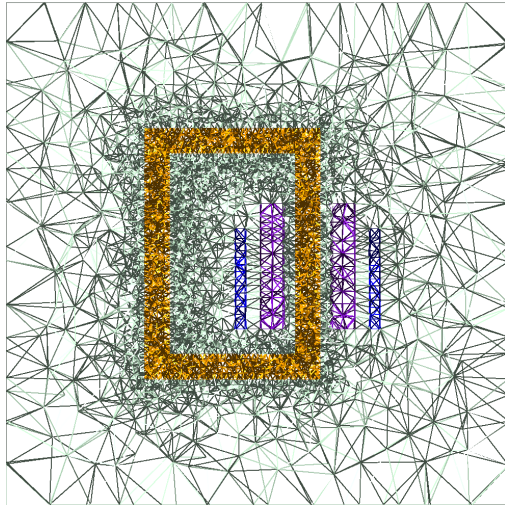
(a) Cross-section of the 3D mesh of the FEM domain Ω_f along the XY-plane. The blue and violet meshes represents the two regions of $\Omega_\star$ where $\|\mathbf{j}\| = 1.05 \cdot 10^6$ and $= 1.25 \cdot 10^6$, respectively. The orange mesh represents the third region of $\Omega_\star$ where $\kappa \sim \nabla \times \mathbf{u}$, which forms a hollow rectangular prism. Local refinement at the edges and corners of this prism is needed because the solution is not smooth there. The green mesh is a hollow rectangular prism with sizes $0.2 \times 0.2 \times 0.15$.

(b) Cross-section of the ℓ^2-norm of the numerical solution $\|\mathbf{u_n}\|_2$ on the FEM domain Ω_f along the XY-plane. Colors are in logarithmic scale. Plot obtained with the multi-field coupling.

FIGURE 4 Mesh and result of the magnetostatic inductor experiment.

5 | CONCLUSIONS

Among the four coupling approaches presented in Section 3, we recommend the PDE-constrained coupling thanks to its reliability. The multi-field and DG-based coupling methods are less expensive, as they rely on less variables, but both suffer from ill-conditioning when dealing with coarse meshes and high numbers of multipoles. Furthermore, the DG-based coupling requires the additional user input of a penalty parameter.

However, as indicated by the numerical experiments of Section 4, as long as one defines an auxiliary boundary Γ far from the field sources, the number and positions of multipoles do not impact much on the numerical solution.

Future research will involve a full numerical analysis of the coupling approaches for Maxwell's equations and an extension to the time domain.

ACKNOWLEDGMENTS

References

1. Jackson John David. *Classical electrodynamics*. New York, NY: Wiley; 3rd ed.1999.

2. Casati Daniele, Hiptmair Ralf. *Coupling Finite Elements and Auxiliary Sources*. Submitted to Computers & Mathematics with Applications; 2018.

3. Smajic Jasmin, Hafner Christian, Leuthold Jürg. Coupled FEM–MMP for Computational Electromagnetics. *IEEE Transactions on Magnetics*. 2016;52(3):1–4.

4. Hafner Christian. *Beiträge zur Berechnung der Ausbreitung elektromagnetischer Wellen in zylindrischen Strukturen mit Hilfe des "Point-Matching"-Verfahrens*. 1980.

5. Mie Gustav. Elektrische Wellen an zwei parallelen Drähten. *Annalen der Physik*. 1900;307:201–249.

6. Vekua Il'ja Nestorovič. *New methods for solving elliptic equations*. North Holland Publishing Company; 1967.

7. Barrera R. G., Estevez G. A., Giraldo J.. Vector spherical harmonics and their application to magnetostatics. *European Journal of Physics*. 1985;6(4):287.

8. Monk Peter. *Finite Element Methods for Maxwell's Equations.* Clarendon Press; 2003.

9. Nédélec Jean-Claude. Mixed finite elements in $\mathbb{R}^3$. *Numerische Mathematik.* 1980;35(3):315–341.

10. Brezzi Franco, Marini Luisa Donatella. A Three-field Domain Decomposition Method. In: Contemp. Math., vol. 157: Amer. Math. Soc., Providence, RI 1994 (pp. 27–34).

11. Popp A., Wohlmuth B. I., Gee M. W., Wall W. A.. Dual Quadratic Mortar Finite Element Methods for 3D Finite Deformation Contact. *SIAM Journal on Scientific Computing.* 2012;34(4):B421-B446.

12. Casagrande Raffael, Winkelmann Christoph, Hiptmair Ralf, Ostrowski Joerg. DG Treatment of Non-conforming Interfaces in 3D Curl-Curl Problems. In: Mathematics in Industry, vol. 23: Cham: Springer International Publishing 2016 (pp. 53–61).

13. Stenberg Rolf. *Mortaring by a method of J.A. Nitsche.* Computational mechanics; 1998.

14. COMSOL Inc. *COMSOL Multiphysics v5.3a.* https://www.comsol.com/; 2017.

15. Geuzaine Christophe, Remacle Jean-François. *Gmsh v3.0.6.* http://gmsh.info/; 2017.

16. Guennebaud Gaël, Jacob Benoît. *Eigen v3.3.4.* http://eigen.tuxfamily.org; 2017.

17. Casagrande Raffael, Winkelmann Christoph. *Hybrid Discontinuous Finite Elements for Power Devices.* ABB Corporate Research Center; 2016.

18. Petra Cosmin Gheorghita, Schenk Olaf, Anitescu Mihai, Lubin Miles, Gärtner Klaus. *PARDISO v5.0.0.* https://www.pardiso-project.org/; 2014.